TAS Journal, vol. 2, n. 3, p. 139
ISSN 2595-1521
SETEMBRO 2018
ranser64@yahoo.com.br

Dynamics analysis of a single cylinder hermetic reciprocating compressor

Rangel SC *§, Navarro HA "in memoriam" § and Cabezas-Gómes L §

** Instituto Federal de Educação Ciência e Tecnologia de São Paulo, Araraquara, Brazil. § Department of Mechanical Engineering, São Carlos School of Engineering, University of São Paulo, São Carlos, Brazil.*

Abstract. This paper describes a dynamic modelling of a hermetic compressor pump. The pump suspension system stiffness matrix is calculated with the suspension springs, taking into account the compressive, flexural and shearing rigidities of the springs. The model allows computing the dynamic, normalized modal, and characteristic frequency matrices, and also the displacement vector of the pump and the overall kinetic and elastic potential energies of the system due to shaking forces. The results include the dynamic behavior of a compressor pump showing time history displacements, rotations and resonance frequencies for a baseline configuration. It is also show the influence of the spring stiffness and positions, through parametric and optimization analyses.

Keywords. *Dynamic analysis, Hermetic reciprocating compressor.*

Introduction. The perishable food conservation depends on keeping them at low temperatures through refrigeration, whether at market points, when they are being transported or in the residences. The most common form of cooling is through the steam compression cycle, where the vapor is compressed, and subsequently has its pressure decreased so that the fluid can evaporate at low pressure as in (1). This is done using a hermetic circuit containing a condenser, an expansion valve or capillary tube, an evaporator and a compressor. The refrigerant gas compression is made by a compressor, which in most cases is the reciprocating or also called alternative type. The compressor that was studied is the idealized refrigeration reciprocating hermetic compressor, not belonged to none manufacturer. The refrigeration reciprocating hermetic compressor is normally composed of three main assemblies of parts named: mechanical assembly, electrical motor and housing. A dynamics model of reciprocating hermetic compressor mechanical parts was made by (2). The authors presented the crankshaft bearing surfaces pressure distributions and orbits behavior. They also detailed some parameters as maximum fluid film pressure, minimum fluid film thickness and maximum vibrations levels. The analysis of the loads in the visco-elastic bearings in a dynamic model of a reciprocating refrigeration compressor was performed by (3). The model includes gyroscopic interactions due to the radial movements of the bearings. The analysis using Newton-Euler method describes the system movement and orbital displacements of the bearings. The author of reference (4) developed a

model to make the computational simulation of the suspension system vibrations of a two-cylinder reciprocating compressor and calculate the response of this rigid system of six degrees of freedom. Reference (5) authors purposed a computational and experimental study on the dynamics characteristics of a planar multi-body mechanical system with joint clearance. The contact-impact model describes the response between journal and bearing considering energy loss. The researches of reference (6) presented a study of the dynamic behavior of the crankshaft of rotary compressors of one and two cylinders. They investigate the influence of the counterweights on the reliability of the rotor system. In the work of reference (7), the authors proposed the procedure that is based on a numerical approach using rotor dynamics theory coupled with the finite element method and the influence coefficients. They showed that to reduce the vibration level of both rotor and stator requires a balancing procedure using objective planes in the rotor and stator. The researchers of reference (8) made a reliable model of finite elements for the balance to the compressor taking into account the behavior of three main mechanical subassemblies: the hermetic housing, the crankcase and the rotor-crankshaft assembly. The authors describe that the experiments carried out show that this multi-stage balancing procedure is much more efficient than the classical approach based only on the dynamic balancing of the rotor-crankshaft assembly. The reference (9) author studied the reduction of vibration and noise caused during compressor operation. He studied a reciprocating one- and two-cylinder refrigerant compressor for refrigeration and air conditioning applications. The author investigates the agitation force due to the reciprocating mass at high frequencies. The study of a rotary type compressor air conditioning application done by (10) analyzes the vibration of the compressor theoretically and experimentally. The authors conclude that in steady state the rotating parts rotate in a medium rotation with fluctuations as a sine curve and the stationary parts vibrate around the center line of the crankshaft axis as a cosine curve. A reverse design optimization method for the procedure of developing a vibration transmission element was developed by (11). The authors proposed a methodology to optimize the reduction of vibration transmission of the discharge shockloop of a linear refrigeration compressor. In this research, the authors attempted to determine the configurations of the transmission element (shockloop) which minimizes vibration in the evaluation position (compressor housing) by reversing the standard approach. A finite element model of a reciprocating hermetic compressor for noise prediction applications was developed by (12). The development of the finite element model of the complete compressor is made in two stages: 1- modeling of the compressor housing and 2- modeling of the assembly of the components within the compressor assembly. The model can be used to predict velocity responses on the face of the housing, with the forces generated internally as excitation. The velocity response data is used directly in the noise prediction. The researchers of reference (13), taking into account the theory of spatially curved bars and the transfer matrix method, performed an axial static load dependence linearly free vibration analysis of cylindrical helical springs.

This paper presents the dynamics modelling of the mounted assembly that goes inside the compressor housing. The housing is not part of the study model in this work. The compressor under study is an alternative type with one cylinder, which uses the slide crank mechanism. The imbalances of masses of components of this mechanism generate shaking forces that contribute

TAS Journal, vol. 2, n. 3, p. 141
ISSN 2595-1521
SETEMBRO 2018
ranser64@yahoo.com.br

to the increase of the noise emission during the operation of the compressor. The compressor used in this study is idealized, with simple shapes and straight lines. The assembly of mechanical system with the electrical motor, shockloop and the suspension springs is called compressor pump assembly or frame, or simply pump (Fig. 1).

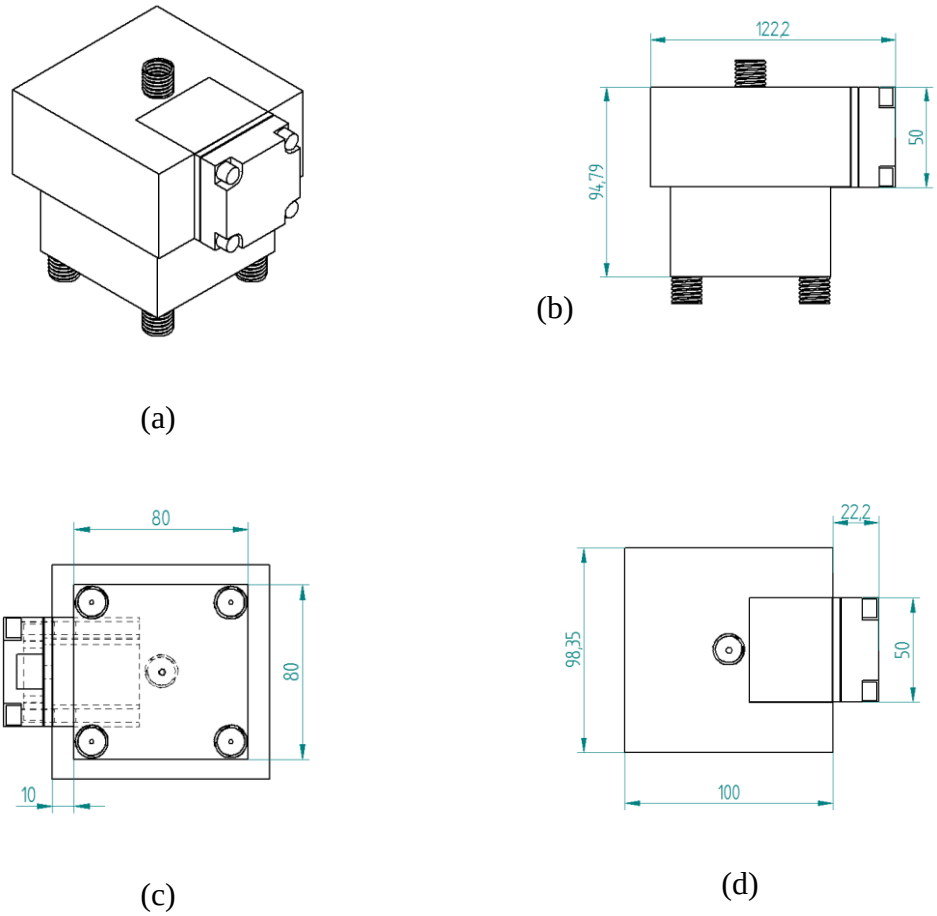

(a) (b) (c) (d)

Figure 1: Mechanical assembly – pump: (a) perspective view; (b) lateral view; (c) lower view; (d) upper view

Dynamics Modelling. The reciprocating compressor uses the slid crank mechanism in its operation. For the application of this mechanism in the compressor, an electric motor is used to drive the crankshaft, in which the force will be transmitted through the connecting rod by driving the piston to compress the gas. Fig. 2(a) shows the simplified design of a four-bar slid crank mechanism. Link 1 is the crankcase with grounding, link 2 is the crankshaft, link 3 is the connecting rod, and link 4 is the slider, which in this case is the piston that is sliding along the cylinder compressing the working fluid.

TAS Journal, vol. 2, n. 3, p. 142
ISSN 2595-1521
SETEMBRO 2018
ranser64@yahoo.com.br

The displacement, velocity and acceleration equations of the sliding piston are described below. According to (14), the displacement *x* of the sliding piston (link 4) taking as reference the top dead center (TDC), showed in Fig. 2(b), is expressed by:

$$x = (R + L) - (Rcos\theta + Lcos\phi) \quad (1)$$

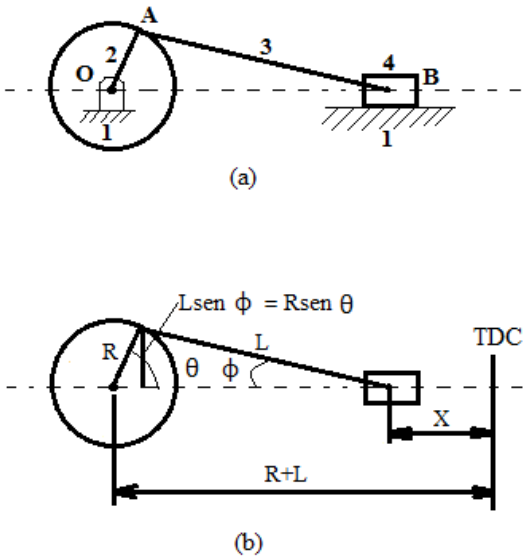

Figure 2: The slider crank mechanism: (a) simple layout of the mechanism; (b) piston displacement with respect to top dead center (TDC) (adapted from (9)).

After some manipulations and simplifications the displacement *x* can be written as:

$$x = R(1 - cos\theta) + \frac{R^2}{2L} sen^2\theta \quad (2)$$

The linear velocity and acceleration of the sliding piston are obtained from Eq. 2, as follow:

$$v = R\Omega \left[sen\theta + \frac{R}{2L} sen2\theta \right] \quad (3)$$

$$a = R\Omega^2 \left[cos\theta + \frac{R}{L} cos2\theta \right] \quad (4)$$

In the above equations $\theta = \Omega t$ where Ω is constant pump angular velocity.

Design views of the compressor pump are shown in Fig. 1. The inertial coordinate system is placed in the equilibrium position of the center of gravity of the pump. The compressor is modeled as a rigid body and the Newton-Euler motion equations for external force in the matrix form results in:

TAS Journal, vol. 2, n. 3, p. 143
ISSN 2595-1521
SETEMBRO 2018
ranser64@yahoo.com.br

$$\bar{\bar{M}}\ddot{\vec{x}} + \bar{\bar{K}}\vec{x} = \vec{F}(t) \tag{5}$$

where $\bar{\bar{M}}$ is the mass and inertia matrix of the system, $\bar{\bar{K}}$ is the total stiffness matrix, $\vec{F}(t)$ represents the vector of the forces and moments, and $\vec{x}$ is the linear and angular displacement vector of the center of gravity of the pump:

$$\vec{x}^T = \left[x, y, z, \theta_x, \theta_y, \theta_z\right]^T \tag{6}$$

The mass and inertia matrix highlights the mass and inertia properties of the compressor assembly. It has both the translation and rotation terms of the pump. The mass (m) and inertia (I) matrix of the system can be written as:

$$\bar{\bar{M}} = \begin{bmatrix} m & 0 & 0 & 0 & 0 & 0 \\ 0 & m & 0 & 0 & 0 & 0 \\ 0 & 0 & m & 0 & 0 & 0 \\ 0 & 0 & 0 & I_{xx} & -I_{xy} & -I_{xz} \\ 0 & 0 & 0 & -I_{yx} & I_{yy} & -I_{yz} \\ 0 & 0 & 0 & -I_{zx} & -I_{zy} & I_{zz} \end{bmatrix} \tag{7}$$

Fig. 3 shows a scheme for each helical compression spring and also for shockloop. This scheme has six degrees of freedom in a three-dimensional space consisting of three translation springs and three spring of rotation in the directions and around the x, y and z axes, respectively.

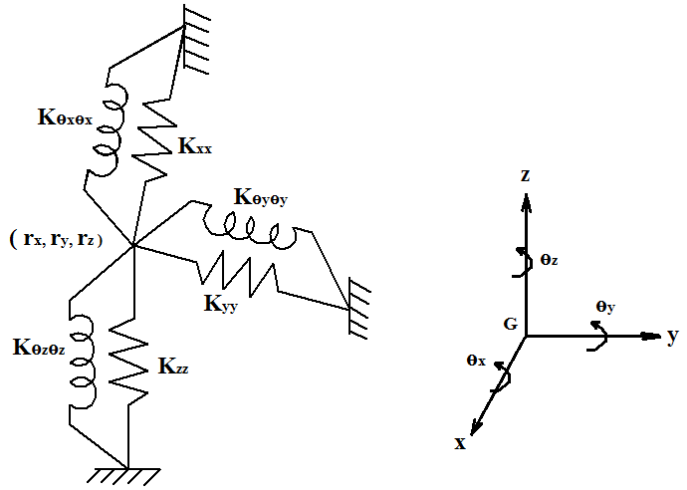

Figure 3: Six degree of freedom of the spring in a three-dimensional space (Adapted from (4))

TAS Journal, vol. 2, n. 3, p. 144
ISSN 2595-1521
SETEMBRO 2018
ranser64@yahoo.com.br

It was adopted for the compressor assembly, a three dimensional coordinate system, where the origin of this coordinate system is located in the center of mass of this assembly (Fig. 4). Fig. 4 also illustrates the position of the center of gravity, the spring forces, the shockloop force, the pump weight force and the piston force.

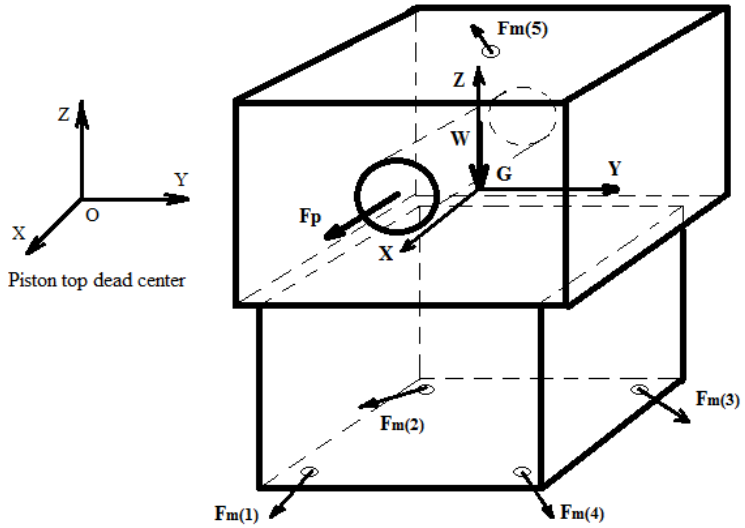

Figure 4: Location of the coordinate axis system

The helical springs (i=1 ,2, 3, 4) and shockloop (i=5) take in account the linear and angular deformations. The stiffness matrix, $\vec{\mathrm{K}}^{(\mathrm{i})}$, is:

$$\bar{\bar{K}}^{(i)} = \begin{bmatrix} K_{xx} & 0 & 0 & 0 & r_z K_{xx} & -r_y K_{xx} \\ 0 & K_{yy} & 0 & -r_z K_{yy} & 0 & r_x K_{yy} \\ 0 & 0 & K_{zz} & r_y K_{zz} & -r_x K_{zz} & 0 \\ 0 & -r_z K_{yy} & r_y K_{zz} & K_{\theta x\theta x} + r_y^2 K_{zz} + r_z^2 K_{yy} & -r_x r_y K_{zz} & -r_x r_z K_{yy} \\ r_z K_{xx} & 0 & -r_x K_{zz} & -r_x r_y K_{zz} & K_{\theta y\theta y} + r_z^2 K_{xx} + r_x^2 K_{zz} & -r_y r_z K_{xx} \\ -r_y K_{xx} & r_x K_{yy} & 0 & -r_x r_z K_{yy} & -r_y r_z K_{xx} & K_{\theta z\theta z} + r_y^2 K_{xx} + r_x^2 K_{yy} \end{bmatrix} \quad (8)$$

$\mathrm{r_x}, \mathrm{r_y}, \mathrm{r_z}$ stand for the position of each spring relative to the center of mass in x, y and z coordinates. For more details about calculations see reference (15). The normalized equation form is obtained as:

$$\ddot{\vec{y}}(t) + \bar{\bar{K}}_g^* \vec{y}(t) = \bar{\bar{M}}_g^{-1} \vec{g}(t) \quad (9)$$

TAS Journal, vol. 2, n. 3, p. 145
ISSN 2595-1521
SETEMBRO 2018
ranser64@yahoo.com.br

Considering the particular case of a harmonic force with amplitude g_0 and frequency Ω, that is, $g(t) = g_0 cos(\Omega t)$ represents the following equation for one-dimensional undamped forced oscillator:

$$\ddot{y}(t) + \omega^2 y(t) = {}^{g_0}/_{m}\, cos(\Omega t) \quad (10)$$

where the particular solution of Eq. 10 is expressed by:

$$y(t) = \frac{{}^{g_0}/_{m}\cos(\Omega t)}{(\omega^2 - \Omega^2)} \quad (11)$$

Considering $\omega^2 = {}^{k}/_{m}$ the amplitude y_0 is given by:

$$y_0 = \frac{g_0/k}{1 - \frac{m\Omega^2}{k}} \quad (12)$$

The kinetic energy is expressed by:

$$KE = \frac{1}{2}[\Omega\vec{x}]^T \bar{\bar{M}}[\Omega\vec{x}] = \frac{\Omega^2}{2}\vec{x}^T \bar{\bar{M}}\vec{x} \quad (13)$$

The elastic potential energy is given by:

$$PE = \frac{1}{2}\vec{x}^T \bar{\bar{K}}\vec{x} \quad (14)$$

The (16) reference's author discuss the combined lateral and axial load and also on bucking of helical compression springs. Tab. 1 shows the parameters used in the computational program. The table presents data of mass, inertia, geometry, material properties for the pump and helical springs.

Table 1: Data for the computational simulation

Description	Parameter
Angular velocity	Ω = 361 [rad/s]
Piston mass	m_p = 0.089 [kg]
Wrist pin mass	m_{wp} = 0.005 [kg]
Mass of the connecting rod part with reciprocating movement	m_{cr} = 0.013779 [kg]
Reciprocating mass	m_r = 0.10779 [kg]
Distance from the center of the cylinder to the center of mass	b = 0.01741 [m]
Helical spring wire diameter	d =1.2 [mm]
Mean helical spring radius	r =7 [mm]
Modulus of elasticity of the helical spring	E = 206842 [N/mm^2]
Modulus of rigidity of the helical spring	G = 79290 [N/mm^2]
Surface inertia moment of the helical spring	I =0.101788 [mm^4]

TAS Journal, vol. 2, n. 3, p. 146
ISSN 2595-1521
SETEMBRO 2018
ranser64@yahoo.com.br

The mass – inertia matrix was obtained with the mechanical assembly geometry (Fig. 1) using a CAD software. From the CAD model, the values of pump mass-inertia matrix $\bar{\bar{M}}$, are given by:

$$\bar{\bar{M}} = \begin{bmatrix} 6.159 & 0 & 0 & 0 & 0 & 0 \\ 0 & 6.159 & 0 & 0 & 0 & 0 \\ 0 & 0 & 6.159 & 0 & 0 & 0 \\ 0 & 0 & 0 & 0.10618 & 0 & -0.005343 \\ 0 & 0 & 0 & 0 & 0.025819 & 0 \\ 0 & 0 & 0 & -0.005343 & 0 & 0.023880 \end{bmatrix}$$

Considering the values of the properties of helical springs (see Tab. 1), the rigidities springs are determined, and the total stiffness matrix $\bar{\bar{K}}$ is:

$$\bar{\bar{K}} = \begin{bmatrix} 97690 & 0 & 0 & 0 & -3274.7 & 0 \\ 0 & 97690 & 0 & 3274.7 & 0 & -172.9 \\ 0 & 0 & 37450 & 0 & 66.3 & 0 \\ 0 & 3274.7 & 0 & 286.673 & 0 & -5.796 \\ -3274.7 & 0 & 66.3 & 0 & 286.753 & 0 \\ 0 & -172.9 & 0 & -5.796 & 0 & 160.361 \end{bmatrix}$$

The dynamic behavior of the system with time and frequency is obtained solving the normalized modal equation (Eq. 8) and using data from Tab. 1 and mass-inertia and total stiffness matrices values.

The following hypotheses were assumed in the development of the present model: 1 – The hermetic housing has zero movement; 2 – The pump and the parts of the compressor like rotor, crankshaft, connecting rod and piston are assumed to be rigid bodies; 3 – Springs are assumed to be linearly deformable and massless bodies; 4 – The inertial forces of the connecting rod, piston and wrist pin are calculated with respect to their positions relative to the center of mass of the pump.

Results. Considering the above set of input data, defined as baseline, the kinetic and elastic potential energies of the system are: KE = 1.051 J, Eq. 13 and PE = 0.0496 J, Eq. 14, respectively. The kinetic energy is approximately 20 times greater than the elastic potential energy. This energy difference appears because the compressor has only one cylinder reciprocating mass, resulting in a higher pump unbalance. In case of even number of cylinders the pump could be balanced more easily based on these energies values.

Figs. 5 and 6 illustrate the time history of the displacements and rotations, respectively. Fig. 5 shows the displacements in the *x*, *y* and *z* directions (solid, dashed and dotted lines,

TAS Journal, vol. 2, n. 3, p. 147
ISSN 2595-1521
SETEMBRO 2018
ranser64@yahoo.com.br

respectively). It is observed that in the *y* direction the pump does not have movement. In the *x*-direction the pump is excited at the frequency of 361 rad/s, and in the *z* direction the pump moves due to gravitational force with amplitude equal to twice the static displacement. As can be noted the most important movement is in the *x* direction, which varies with the excitation frequency.

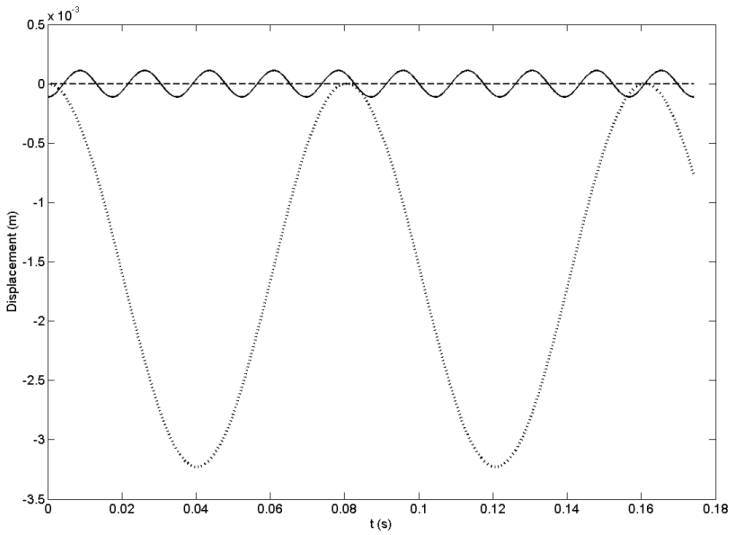

Figure 5: Displacement in *x*, *y* and *z* (solid, dashed and dotted lines) as a function of time

Fig. 6 illustrates the rotation in the *x*, *y*, and *z* directions (solid, dashed and dotted lines, respectively). It is observed that the main rotation occurs around the *y*-axis, θy, in the excitation frequency. However, this vibration is small because the small distance value (b = 0.01741 m) from the cylinder axis up to the center of mass of the compressor pump. This is the expected behavior because regarding the *x* and *z* directions the piston movement is symmetric.

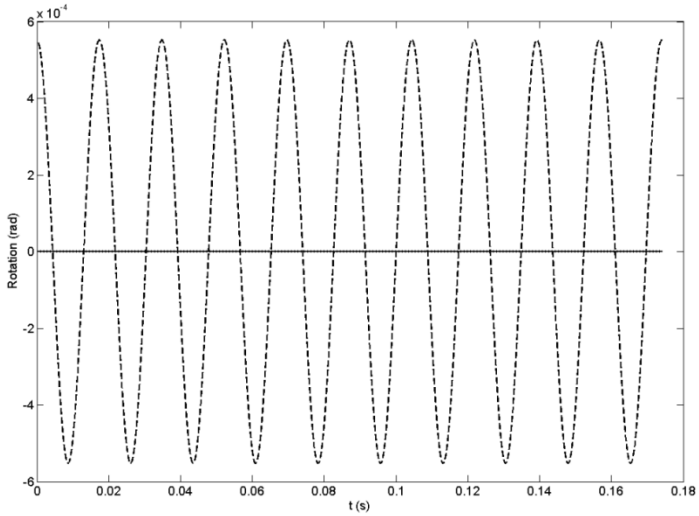

Figure 6: Rotations θx, θy e θz (solid, dashed and dotted lines) as a function of time

TAS Journal, vol. 2, n. 3, p. 148
ISSN 2595-1521
SETEMBRO 2018
ranser64@yahoo.com.br

Next the pump movement is analyzed as a function of excitation frequency variation. Figs. 7, 8 and 9 illustrate system responses as a function of the excitation frequency, varying in the range 0 to 4500 rpm (0 to 471.24 rad/s). Figs. 7 and 8 illustrate the displacement in the *x*-direction and the rotation about the y-axis (θy) as a function of the frequency, respectively. Using the normalized modal matrix $\bar{\bar{P}}$ the generalized physical variables *x* and θy are expressed by:

$$x = 0.085824y1 + 0.048533y2 + 0.043779y3 \quad (15)$$

and

$$\theta y = -0.99631y1 + 0.99878y2 + 0.80413y3 \quad (16)$$

It is observed that for these variables only the first three resonance frequencies dominate the movement, that is, 148.44 rad/s; 70.14 rad/s and 78.07 rad/s. The frequencies of 70.14 rad/s and 78.07 rad/s have less contribution compared to that of 148.44 rad/s. This fact is noted in Figs. 7 and 8, where the first resonance frequency peak of 148.44 rad/s (1417 rpm) is higher than the resonance frequencies peaks of 70.14 rad/s (670 rpm) and 78.07 rad/s (746 rpm). The main cause of this behavior is that the movements are dominated by the linear displacement of the compressor piston in the *x*-direction and by the rotation in the *y*-direction (θy). It should be observed that there are three other resonance frequencies that can be neglected because the system response in these frequencies is negligible. In fact, the system has six degrees of freedom and consequently has six resonance frequencies, but only three of them have to be considered, as can be seen from Figs. 7, 8, and 9.

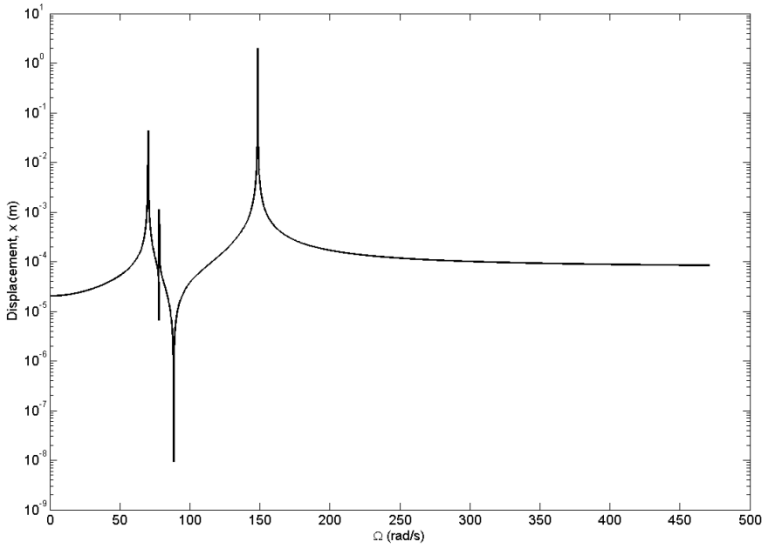

Figure 7: Displacement in the *x* direction as a function of frequency.

TAS Journal, vol. 2, n. 3, p. 149
ISSN 2595-1521
SETEMBRO 2018
ranser64@yahoo.com.br

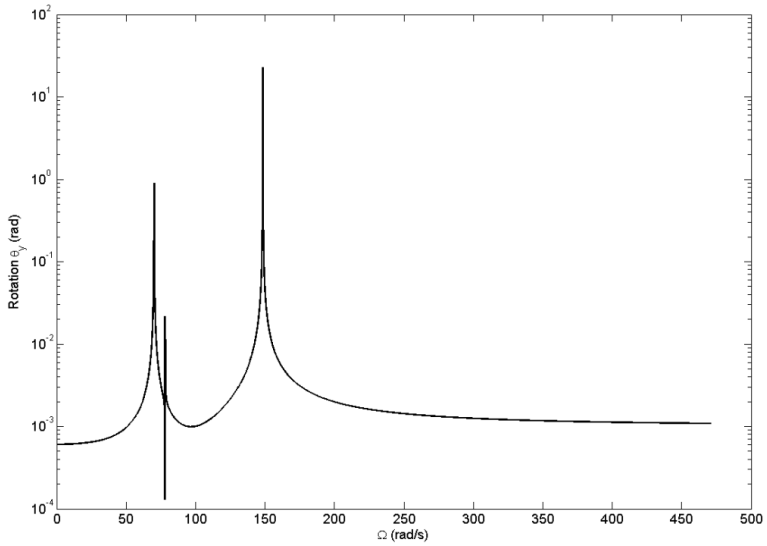

Figure 8: Rotation around the *y* axis (θy) as a function of frequency.

Fig. 9 shows the kinetic, elastic potential and the sum of kinetic and elastic potential energies (solid, dashed and dotted lines, respectively) as a function of the excitation frequency. The kinetic energy is a function of the frequency chancing with it. This also occurs with the sum of elastic potential and kinetic energies. The highest variation of these energies is observed in the first resonance frequency (148.44 rad/s). There are also observed smaller energy variations for the two others resonance frequencies (70.14 rad/s and 78.07 rad/s, respectively).

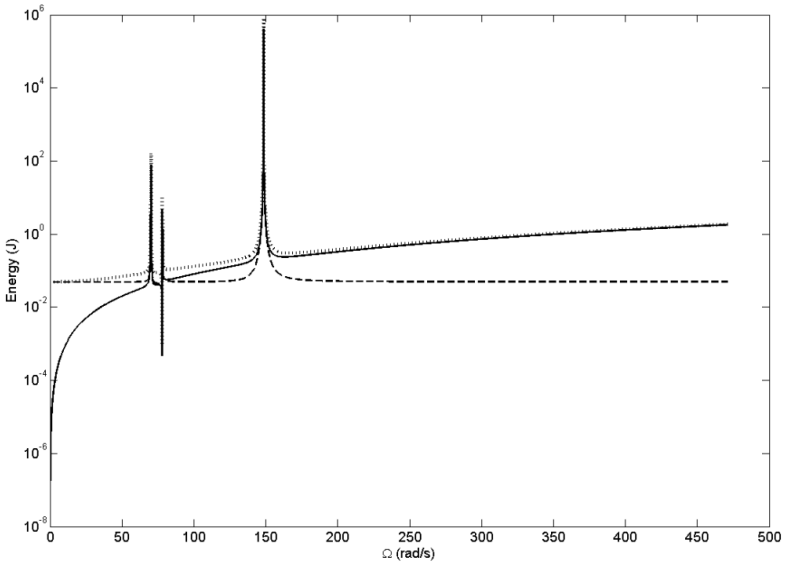

Figure 9: Kinetic, potential and the sum of kinetic and elastic potential energies as a function of frequency (solid, dashed and dotted lines).

Now is presented a parametric study changing the spring compressive and shearing rigidities K_{xx}, K_{yy} and K_{zz}. The following three different conditions are considered increasing the

TAS Journal, vol. 2, n. 3, p. 150
ISSN 2595-1521
SETEMBRO 2018
ranser64@yahoo.com.br

spring stiffness values: condition 1 (K_{xx} = 10000 N/m; K_{yy} = 10000 N/m; K_{zz} = 3700 N/m); baseline (K_{xx} = 19538 N/m; K_{yy} = 19358 N/m; K_{zz} = 7490 N/m); and condition 2 (K_{xx} = 50000 N/m; K_{yy} = 50000 N/m; K_{zz} = 18000 N/m). In all conditions the spring positions and the flexural and torsional spring rigidities values are fixed: $K_{\theta x \theta x} = K_{\theta y \theta y}$ = 1.1551 N.m/rad; $K_{\theta z \theta z} = 0$.

In Tab. 2 are shown resulting values of kinetic and elastic potential energies and resonance frequencies for the assumed three conditions. An increase in the spring stiffness leads to an increase of the resonance frequency and to a decrease of the overall kinetic and potential energies. The overall kinetic energy decreases from 2.95 J to 0.242 J as the spring stiffness condition is changed from condition 1 to 2. The overall elastic potential energy changes from 0.0823 J to 0.0272 J. The first resonance frequency changes from 107.83 rad/s to 235.49 rad/s when the spring stiffness condition is increased from condition 1 to 2.

Table 2: Results from computational simulation of spring stiffness variation

Description	Condition 1	Baseline	Condition 2
KE [J]	2.95	1.051	0.242
PE [J]	0.0823	0.0496	0.0272
Resonance frequency f_1 [rad/s]	107.83	148.44	235.49
Resonance frequency *f2* [rad/s]	66.94	70.14	77.17
Resonance frequency *f3* [rad/s]	60.09	78.07	113.65
Resonance frequency *f4* [rad/s]	143.14	197.28	312.58
Resonance frequency *f5* [rad/s]	85.46	75.97	92.70
Resonance frequency *f6* [rad/s]	57.15	94.27	136.03

Fig. 10 shows the *x*-displacement as a function of frequency for conditions 1 (solid line) and 2 (dotted line), respectively. It is observed higher resonance frequencies for condition 2. Fig. 11 shows the rotations about the *y* axis (θy) as a function of frequency for the conditions 1 (solid line) and 2 (dotted line), respectively. It is also observed that the resonance frequencies increased for condition 2. This expected behavior is caused by the stiffness increase.

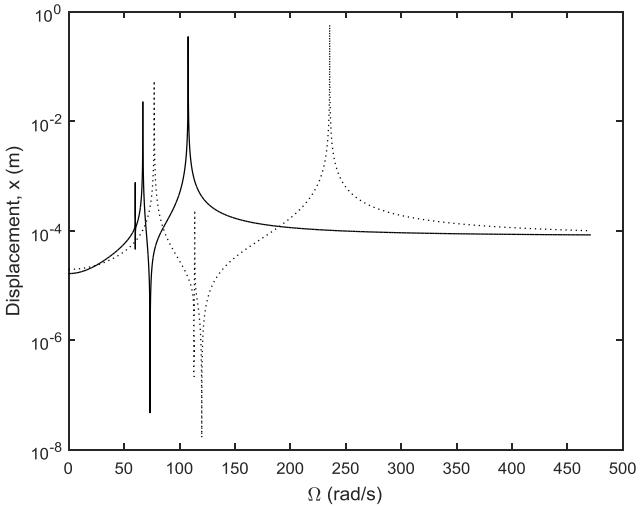

Figure 10 – Displacement in the *x* direction as function of frequency for condition 1 (solid line) and 2 (dotted line).

TAS Journal, vol. 2, n. 3, p. 151
ISSN 2595-1521
SETEMBRO 2018
ranser64@yahoo.com.br

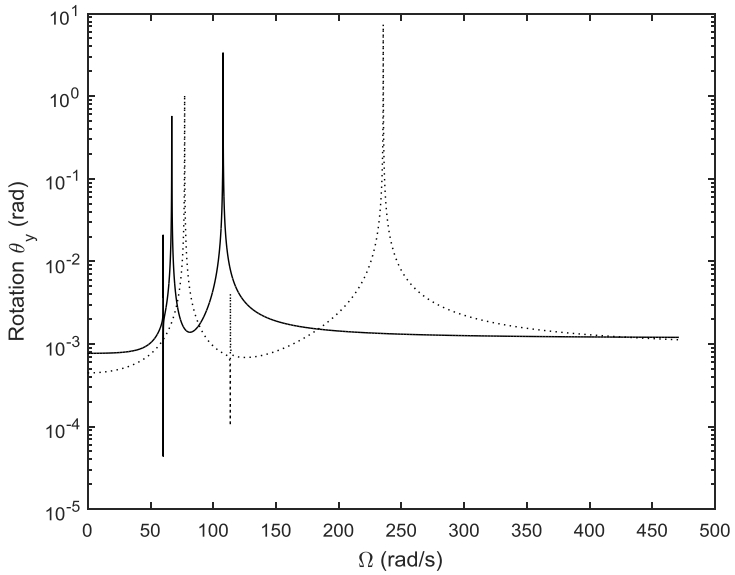

Figure 11 – Rotation around the *y* axis (θy) as function of frequency for condition 1 (solid line) and 2 (dotted line).

Fig. 12 shows the total energy (sum of kinetic and elastic potential energies) as a function of frequency for condition 1 (solid line), baseline (dashed line) and condition 2 (dotted line). Comparing the three curves, it is observed that the frequencies of resonances are moved to the right with the increasing of the spring rigidity (from condition 1 to condition 2). Far from the resonance frequencies, the total energy is decreasing with the increasing of the rigidity. Close to the resonance frequencies, the peaks are very sensible and depend on the numerical refinement frequency.

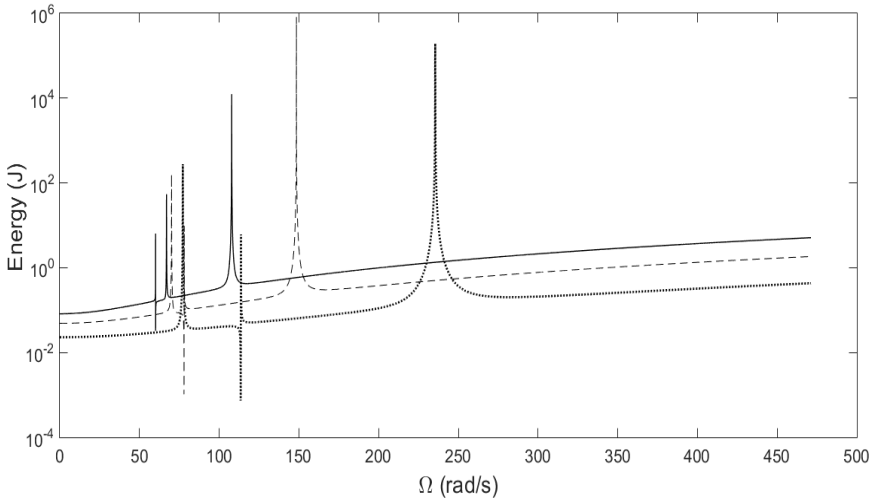

Figure 12 – Sum of the kinetic and the elastic potential energies as a function of frequency: condition 1 (solid line); baseline (dashed line); condition 2 (dotted line).

TAS Journal, vol. 2, n. 3, p. 152
ISSN 2595-1521
SETEMBRO 2018
ranser64@yahoo.com.br

Next is shown an analysis regarding the total energy variation with spring stiffness and position considering the baseline condition. In Fig. 13 is shown the total energy variation as a function of compressive rigidity K_{zz} in axial *z* direction. This curve was obtained through the use of a Matlab constrained nonlinear optimization function "fmincon" (17) applied to the present procedure for total energy calculation. The optimum energy value was searched considering a variation of five rigidities terms with the following lower and upper bounds ($10000 \leq K_{xx}$, $K_{yy} \leq$ 50000 N/m; $3700 \leq K_{zz} \leq 18700$ N/m; $0.5 \leq K_{\theta x \theta x}$, $K_{\theta y \theta y} \leq 5.0$ N.m/rad). The value of $K_{\theta z \theta z} = 0$ was held constant.

Using this optimization function it was found a minimum total energy value (0.245 J) for the higher allowable (upper bound) K_{zz} value equal to 18700 N/m. The obtained results showed that the total energy does not depend on the variation of the rigidity in the other directions, for the considered angular velocity (361 rad/s). In fact in Fig. 5 is shown that for this frequency the highest displacement occurs in *z* direction. As can be noted the total energy present only a quasi linear variation with K_{zz}. The results can change for other values of angular velocity, but it is estimated that will follow the same tendency.

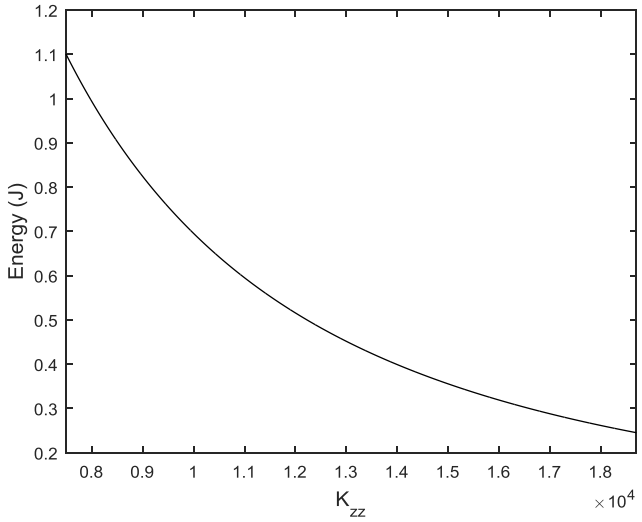

Figure 13 – Total energy (sum of kinetic and elastic potential energies) variation with K_{zz}.

A new total energy optimization is performed using the previous K_{zz} value (18700 N/m) for the obtained minimum total energy. The aim of this analysis is to found a new minimum total energy value as a function of the spring position. In this analysis was considered only the variation of *x* and *y* positions of fifth spring, that is, the spring that acts in the direction of the gravitational force, in the place of the shockloop. The optimum energy value is searched considering the following lower and upper bounds ($-0.01 \leq r_x$, $r_y \leq 0.01$ m) while the value of r_z was held constant to maintain the pump position. All the other input parameters assumed the baseline condition values, including the angular velocity equal to 361 (rad/s).

TAS Journal, vol. 2, n. 3, p. 153
ISSN 2595-1521
SETEMBRO 2018
ranser64@yahoo.com.br

The total energy variation as a function of r_x for the fifth spring is shown in Fig. 14. The same Matlab constrained nonlinear optimization function "fmincon" (17) is used. In this case it was found a truly minimum total energy value of 0.1934 J at the r_x = 0.00413 m *x* coordinate value. It was not found any variation of the total energy with the spring position in the *y* direction, maybe because the main piston movement is in the *x* direction. As noted the variation of r_x leads to a new total energy minimum showing the importance of application of such kind of optimization calculation, in order to minimize the pump oscillations. This minimum value was obtained after previously computing the appropriate value of K_{zz} for the first minimization calculation.

In the case of applying this same optimization considering the baseline rigidity values the minimum total energy increased to values much higher than those initially obtained (0.245 J), indicating the necessity of performing the minimization computations for the above two considered variables. However, multivariable optimizations including more than two variables, for example, including also the angular velocity could be important for obtaining less pump oscillations.

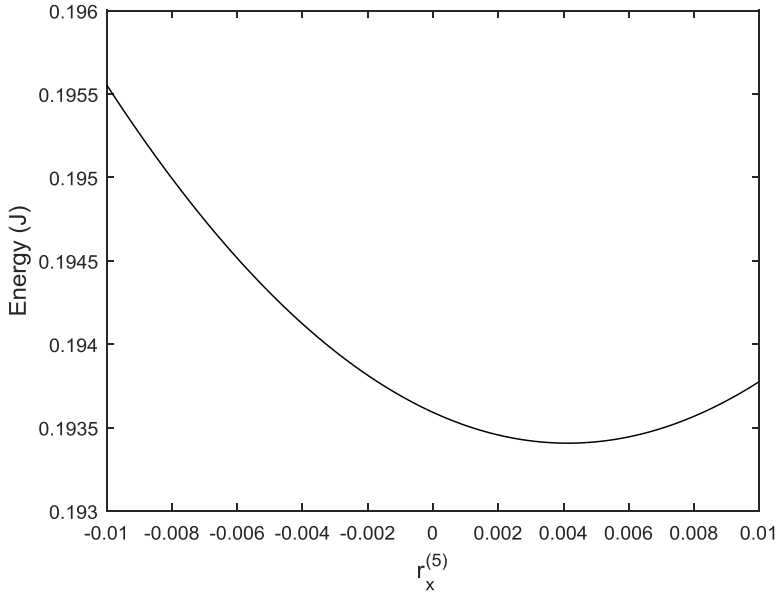

Figure 14 – Total energy (sum of kinetic and elastic potential energies) variation with r_x for the fifth spring.

TAS Journal, vol. 2, n. 3, p. 154
ISSN 2595-1521
SETEMBRO 2018
ranser64@yahoo.com.br

Conclusion. In this work it is performed the dynamic analysis of the compressor pump using an idealized geometric model and the corresponding mathematical model. With this geometrical model it is possible to calculate the total stiffness matrix of the system with the suspension springs, taking into account the compressive, flexural and shearing rigidities of the springs. The calculation of the stiffness matrix together with the mass and inertia matrix of the pump system enable the simulation with the dynamic model.

The solution of the computational model allows computing the dynamic, normalized modal, and characteristic frequency matrices, and also the displacement vector $\vec{x}$ of the mass center of the pump and the overall kinetic (*KE*) and elastic potential (*PE*) energies of the system due to shaking forces. The model allows calculating the behaviors of other dynamic variables as a function of time and frequency. The occurrence of a main resonance frequency of 148.44 rad/s is observed for baseline condition. For the parametric analysis, the total energy decreases as the spring rigidities increase from condition 1 to condition 2. The resonance frequency also increased. Finally two optimization calculations were performed considering the minimization of the total energy. Overall these analyzes pointed out to the augmentation of the K_{zz} values and to an optimum value of the r_x position value of shockloop for obtaining a minimum value of total energy.

The following main conclusions can be addressed:
- The developed computational methodology allows studying a dynamic behavior of a compressor pump aiding to find the resonance frequencies and the influence of the spring stiffness and positions, through parametric and optimization analyses.
- The model finds the main resonance frequency and helps to project the spring stiffness in order to avoid the occurrence of resonance frequencies of the system in the operational range of real compressor speeds.

Acknowledgments. The first author acknowledges the financial supports received from the "Coordenação de Aperfeiçoamento de Pessoal de Nível Superior (CAPES - Brazil)" for a scholarship and the financial supports received from the "Instituto Federal de Educação Ciência e Tecnologia de São Paulo (IFSP- Brazil)". The second and third authors acknowledge the "Conselho Nacional de Desenvolvimento Científico e Tecnológico (CNPq – Brazil)" for financial support (Processes 303476/2015-0 and 304972/2017-7).

Disclosure. The authors report no conflicts of interest in this work.

References.

(1) Stoecker, WF, and Jones, JW. Refrigeração e Ar Condicionado, tradução José M. Saiz Jabardo et. al., Ed. McGraw-Hill do Brasil, São Paulo; 1985.
(2) Estupiñan, EA, Santos, IF. Dynamic modeling of hermetic reciprocating compressors, combining multibody dynamics, finite element method and fluid film lubrication. International Journal of Mechanics, issue 4, volume 1; 2007.
(3) Kurka, PRG, Izuka, JH, Paulino, KLG. Dynamic of reciprocating compressors with flexible bearings. Mechanism and Machine Theory. 2012;52, p.130–143.
(4) Arcot, RP. Computer simulation of the Bristol compressor suspension system dynamics [Thesis]. Virginia Polytechnic institute & State University, Blacksburg; 1993.
(5) Chen, Y, Sun, Y, Peng, B, Cao, C. A comparative study of joint clearance effects on dynamic behavior of planar multibody mechanical systems. Latin American Journal of Solids and structure. 2016;13: 2815-2833.
(6) Wu, J, Zhang, H, Xie, F, Chen, A, Li, Y. Dynamic behaviors of the crankshaft in single-cylinder and twin-cylinder rotary compressors. International Journal of refrigeration. 2014;47 p. 36–45.
(7) Sève, F, Andrianoely, MA, Berlioz, A, Dufour, R, Charreyron, M. Balancing of machinery with a flexible variable-speed rotor. Journal of sound and vibration. 2003;264:287-302.
(8) Levecque, N, Mahfoud, J, Violette, D, Ferraris, G, Dofour, R. Vibration reduction of a single cylinder reciprocating compressor based on multi-stage balancing. Mechanism and Machine Theory. 2011;46, p.1–9.
(9) Ong, CG. Shaking and balance of a convertible one-and two-cylinder reciprocating compressor [Thesis]. Virginia Polytechnic institute & State University, Blacksburg; 2000.
(10) Yanagisawa, T, Mori, M, Shimizu, T, Oji, Y. Vibration of a rolling piston type rotary compressor. International Journal of Refrigeration. 1984;volume 7, number 4.
(11) Wang, S, Lee, J, Hyun, J, Ki, S. Development procedure for a vibration transmission element using a reversed design optimization method. Journal of sound and vibration. 2015;354p.72–85.
(12) Ramani, A. Finite element modeling of a refrigeration compressor for noise predictions applications [Thesis]. Virginia Polytechnic institute & State University, Blacksburg; 1993.
(13) Yildirim, V. Axial static load dependence free vibration analysis of helical springs based on the theory of spatially curved bars. Latin American Journal of Solids and structure. 2016;13:2
(14) Mabie, HH and Reinholtz, CF. Mechanisms and dynamics of machinery. 4a ed., Virginia Polytechnic Institute and State University, John Wiley, Singapore; 1987.
(15) Rangel, SC. Análise por elementos finitos da junta de vedação e dinâmica de um compressor hermético [Thesis]. Department of Mechanical Engineering, São Carlos School of Engineering, University of São Paulo, São Carlos, Brazil; 2017.
(16) Wahl, AM. Mechanical Springs. First Edition, Penton Publishing Company, Cleveland, Ohio; 1944.
(17) Yang, WY, Cao, W, Chung, T-S., Morris, J. Applied Numerical Methods using MATLAB. First Edition, John-Wiley & Sons, Inc., Hoboken, New Jersey; 2005.